Caveolin-1 Null (−/−) Mice Show Dramatic Reductions in Life Span†

David S. Park,[‡,§] Alex W. Cohen,[‡,§] Philippe G. Frank,[§] Babak Razani,[§] Hyangkyu Lee,[§] Terence M. Williams,[§] Madhulika Chandra,[∥] Jamshid Shirani,[∥,⊥] Andrea P. De Souza,[#] Baiyu Tang,[#] Linda A. Jelicks,[#] Stephen M. Factor,[⊥,△] Louis M. Weiss,[⊥,△] Herbert B. Tanowitz,[⊥,△] and Michael P. Lisanti*[,§]

Department of Molecular Pharmacology, Albert Einstein College of Medicine, Divisions of Cardiology and Infectious Disease, Department of Medicine, Albert Einstein College of Medicine and The Montefiore Medical Center, Department of Pathology, Albert Einstein College of Medicine, Department of Physiology and Biophysics, Albert Einstein College of Medicine, and Department of Medicine, Albert Einstein College of Medicine, 1300 Morris Park Avenue, Bronx, New York 10461

Received September 10, 2003; Revised Manuscript Received October 23, 2003

ABSTRACT: Caveolae are 50−100 nm flask-shaped invaginations of the plasma membrane found in most cell types. Caveolin-1 is the principal protein component of caveolae membranes in nonmuscle cells. The recent development of Cav-1-deficient mice has allowed investigators to study the in vivo functional role of caveolae in the context of a whole animal model, as these mice lack morphologically detectable caveolae membrane domains. Surprisingly, Cav-1 null mice are both viable and fertile. However, it remains unknown whether loss of caveolin-1 significantly affects the overall life span of these animals. To quantitatively determine whether loss of Cav-1 gene expression confers any survival disadvantages with increasing age, we generated a large cohort of mice ($n = 180$), consisting of Cav-1 wild-type (+/+) ($n = 53$), Cav-1 heterozygous (+/−) ($n = 70$), and Cav-1 knockout (−/−) ($n = 57$) animals, and monitored their long-term survival over a 2 year period. Here, we show that Cav-1 null (−/−) mice exhibit an ∼50% reduction in life span, with major declines in viability occurring between 27 and 65 weeks of age. However, Cav-1 heterozygous (+/−) mice did not show any changes in long-term survival, indicating that loss of both Cav-1 alleles is required to mediate a reduction in life span. Mechanistically, these dramatic reductions in life span appear to be secondary to a combination of pulmonary fibrosis, pulmonary hypertension, and cardiac hypertrophy in Cav-1 null mice. Taken together, our results provide the first demonstration that loss of Cav-1 gene expression and caveolae organelles dramatically affects the long-term survival of an organism. In addition, aged Cav-1 null mice may provide a new animal model to study the pathogenesis and treatment of progressive hypertrophic cardiomyopathy and sudden cardiac death syndrome.

First implicated in the uptake of small and large molecules via transcytosis and potocytosis, caveolae are now known to play a role in numerous cellular processes. Some of these include cholesterol (*1*−*3*) and triglyceride homeostasis (*4*−*6*), cell cycle regulation (*7*, *8*), apoptosis (*9*), and the regulation of signal transduction pathways (*10*). The broad functional range of these plasmalemmal organelles is attributable to two properties of caveolae membranes: (i) their unique lipid composition and (ii) the structural proteins of caveolae, known as caveolins.

Caveolae are specialized membrane domains highly enriched in sphingolipids and cholesterol (*11*−*14*). This unique lipid composition confers upon these membranes resistance to solubilization by nonionic detergents at low temperatures and a buoyant density during sucrose gradient ultracentrifugation (*12*). Utilizing various isolation techniques, numerous researchers have identified a host of signal transduction molecules (Src-family tyrosine kinases, H-Ras, eNOS,[1] and heterotrimeric G-proteins) that reside in caveolae membrane domains (*15*). Fatty acylation may represent a common mechanism by which cytoplasmic signaling molecules are targeted to caveolae (*16*−*19*).

The principal structural proteins of caveolae are encoded by the caveolin gene family (caveolin-1, -2, and -3). Caveolin-1 and -2 are coexpressed in numerous tissue types, with particularly high expression in adipocytes, endothelial cells, fibroblasts, and epithelial cells. Caveolin-3, on the other hand, is muscle-specific, being highly expressed in skeletal, cardiac, and smooth muscle cells. It has been proposed that

† This work was supported by grants from the National Institutes of Health (NIH), the Muscular Dystrophy Association (MDA), the Susan G. Komen Breast Cancer Foundation, and the American Heart Association (AHA), as well as by a Hirschl/Weil-Caulier Career Scientist Award (all to M.P.L.). D.S.P. was supported by an NIH Graduate Training Program Grant (TG-CA09475). B.R., A.W.C., and T.M.W. were supported by an NIH Medical Scientist Training Grant (T32-GM07288). P.G.F. was recipient of a Scientist Development Grant from the AHA. H.B.T. was supported by a grant from the NIH (AI-12770).

* Corresponding author. Tel: (718) 430-8828. Fax: (718) 430-8830. E-mail: lisanti@aecom.yu.edu.

‡ Contributed equally and should be considered co-first authors.

§ Department of Molecular Pharmacology, Albert Einstein College of Medicine.

∥ Divisions of Cardiology and Infectious Disease, Department of Medicine, Albert Einstein College of Medicine and The Montefiore Medical Center.

⊥ Department of Pathology, Albert Einstein College of Medicine.

Department of Physiology and Biophysics, Albert Einstein College of Medicine.

△ Department of Medicine, Albert Einstein College of Medicine.

[1] Abbreviations: Cav-1, caveolin-1; eNOS, endothelial nitric oxide synthase; Het, heterozygous; KO, knockout; LV, left ventricle; MRI, magnetic resonance imaging; PBS, phosphate-buffered saline; RV, right ventricle.

10.1021/bi0356348 CCC: $25.00 © 2003 American Chemical Society
Published on Web 12/05/2003

caveolin family members function as scaffolding proteins (*20*) to organize and modulate the activity of lipid-modified signaling molecules (*21*−*24*) within caveolae membranes. In support of this hypothesis, caveolin-1 binding can functionally suppress the GTPase activity of heterotrimeric G-proteins (*21*) and inhibit the kinase activity of Src-family tyrosine kinases and receptor tyrosine kinases through a common protein domain, termed the caveolin-scaffolding domain (*24*−*27*).

Historically, caveolin-1 was first identified as a major tyrosine phosphorylated protein in v-Src-transformed chick embryo fibroblasts. On the basis of their observations, Glenney and colleagues proposed that caveolin-1 may serve as a critical mediator of cellular transformation (*28*). Multiple lines of evidence now support the hypothesis that caveolin-1 acts as a tumor suppressor gene: (i) caveolin-1 expression is highest in terminally differentiated cells (*29*) and absent in oncogenically transformed cell lines (*30*, *31*), (ii) caveolin-1 downregulation induces oncogenic transformation in NIH-3T3 cells (*32*) while reexpression of caveolin-1 in breast cancer cell lines inhibits tumor growth (*33*, *34*), (iii) caveolin-1 induces G_0/G_1 arrest through a p53/p21-dependent pathway (*8*), and (iv) the CAV-1 gene has been localized to a suspected tumor suppressor locus in mice (6-A2) and humans (7q31) that is deleted in many forms of cancer (*35*, *36*).

Mutations in the caveolin gene family have now been identified in various human diseases. Examination of 92 primary human breast cancer samples yielded a mutation in CAV-1 at codon 132 (P132L) in 16% of the cases, with invasive scirrhous carcinomas being the most frequent type of cancer associated with this mutation (*37*). A similar proline to leucine (P104L) mutation was also identified in the CAV-3 gene in patients with limb girdle muscular dystrophy (*38*). Interestingly, both CAV-1 and CAV-3 mutations behave in a dominant-negative fashion, causing the intracellular retention of wild-type caveolins at the level of the Golgi complex (*39*, *40*).

The recent generation of Cav-1 deficient mice by several laboratories has proven an invaluable tool in understanding the functional role of caveolae in mammalian physiology. Surprisingly, young Cav-1 null mice are both viable and fertile. However, by 2−4 months of age, loss of Cav-1 results in cardiovascular abnormalities (*41*−*43*), pulmonary hypertension (*42*), defects in lipid metabolism and adipocyte homeostasis (*5*, *44*), and the hyperproliferation of epithelial and endothelial cells (*27*, *39*, *45*, *46*). These diverse abnormalities underscore the functional versatility of Cav-1 in multiple organ systems in vivo. However, it remains unknown whether loss of caveolin-1 significantly affects the overall life span, i.e., the long-term survival, of these animals.

To investigate whether the loss of Cav-1 confers a signficant survival disadvantage, a cohort of 180 mice, consisting of Cav-1 (+/+), Cav-1 (+/−), and Cav-1 (−/−) animals, were observed over a 2 year period. Interestingly, we show here that Cav-1 null (−/−) mice exhibited an ∼50% reduction in life span at the end of 2 years, with the major declines in viability occurring between 27 and 65 weeks of age. We propose that these mice die either from severe right-sided heart failure secondary to pulmonary hypertension (cor pulmonale) or from an acute arrythmia secondary to hypertrophic cardiomyopathy. These data provide the first demonstration that loss of Cav-1 gene expression dramatically affects the in vivo long-term survival of an organism.

MATERIALS AND METHODS

Animal Studies. All animals were housed and maintained in a barrier facility at the Institute for Animal Studies, Albert Einstein College of Medicine. Cav-1 WT (+/+), Cav-1 Het (+/−), and Cav-1 KO (−/−) mice were generated by interbreeding Cav-1 Het (+/−) mice (*45*) that were in a C57Bl/6 background. Upon weaning, male and female mice were separated into different cages. All mice in this study remained sexually inactive throughout the study.

Preparation of Tissue Paraffin Sections. Mice were checked twice daily. Mice that were found dead were immediately recorded and their internal organs were removed and placed in 10% formalin. The tissue was fixed for ∼24 h, washed in PBS for 20 min, and dehydrated through a graded series of ethanol washes (at room temperature). The tissue samples were then treated with xylene for 40 min (at room temperature) and then incubated with paraffin for 1 h at 55 °C. Paraffin-embedded 5 μm thick sections were prepared using a Microm (Baxter Scientific) microtome and placed on super-frost plus slides (Fisher). Slides were then stained with hematoxylin and eosin (H and E), according to standard laboratory protocols. For cardiac specimens, areas of the myocardium (left ventricle and intraventricular septum) were selected for imaging. For adipose specimens, perigonadal fat pads were used. For lung samples, an 18 gauge syringe was inserted into the trachea, and lungs were filled with 10% formalin. Samples were then examined in a blinded fashion by an expert cardiopathologist (Dr. Stephen M. Factor).

Gated Cardiac Magnetic Resonance Imaging. MRI experiments were performed using a GE Omega 9.4T vertical bore MR system equipped with a microimaging accessory and custom-built coils designed specifically for mice. Just prior to each image acquisition, the heart rate was determined from the ECG, and the spectrometer gating delay was set to acquire data in diastole and systole. Multislice spin−echo imaging with an echo time of 18 ms and a repetition time of approximately 100−200 ms was performed. A 35 mm field of view (with a 256 × 256 pixel image matrix) was used. Short and long axis images of the heart were acquired, and MRI data were processed off-line with MATLAB-based custom-designed software.

Transthoracic Echocardiography. Transthoracic echocardiography was performed on 12-month-old mice, as follows. Echocardiography was performed with mice in the supine position on a heating pad set at 38 °C. Light anesthesia was achieved using an intraperitoneal injection of chloral hydrate (300 mg/kg). Continuous, standard electrocardiograms were taken from electrodes placed on the extremities. Echocardiographic images were obtained using an annular array, broad-band, 10/5 MHz transducer attached to an HDI 5000 CV ultrasound system (Advanced Technology Laboratories, Bothel, WA). A small gel standoff was placed between the probe and chest. Two-dimensional and M-mode images of the heart were obtained from the basal short axis view of the heart and stored on $^3/_4$ in. SVHS videotapes for off-line measurements using the Nova-Microsonic (Kodak) Imagevue DCR workstation (Indianapolis, IN). All measurements were

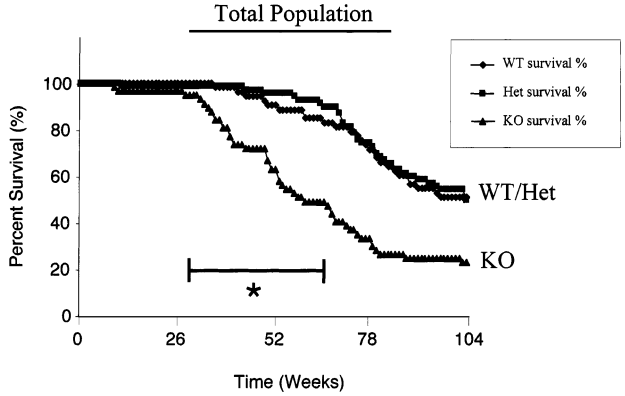

FIGURE 1: Kaplan−Meier survival curve of Cav-1 WT, Het, and KO mouse cohorts. A cohort of 180 mice, consisting of Cav-1 WT (+/+) ($n = 53$), Cav-1 Het (+/−) ($n = 70$), and Cav-1 KO (−/−) ($n = 57$) animals, was observed over a 2 year period. Note that Cav-1 null (−/−) mice exhibited an ∼50% reduction in viability at the end of 2 years, with major declines in viability occurring between 27 and 65 weeks (see asterisk). However, Cav-1 Het (+/−) mice did not show any changes in long-term survival, indicating that loss of both Cav-1 alleles is required to mediate a reduction in life span.

made in three to six consecutive cardiac cycles, and the averaged values were used for analysis. Left ventricular end-diastolic and end-systolic diameters, as well as diastolic ventricular septal and posterior wall thickness, were measured from M-mode tracings. Diastolic measurements were performed at the point of greatest cavity dimension, and systolic measurements were made at the point of minimal cavity dimension, using the leading edge method of the American Society of Echocardiography (*47*). Additionally, the following parameters were calculated using the above-mentioned measurements: left ventricular diastolic wall thickness as the average of ventricular septal and left ventricular posterior wall thickness; left ventricular percent fractional shortening as 100[(end-diastolic diameter minus end-systolic diameter)/(end-diastolic diameter)]; and relative wall thickness as 2(left ventricular diastolic wall thickness)/(end-diastolic diameter).

Note that differences between the absolute wall thickness measured using MRI and echocardiography are commonly observed and are likely due to technical factors, such as differences in the time of gating.

RESULTS AND DISCUSSION

Quantitation of Longevity. The goal of this study was to examine whether the cumulative defects in Cav-1 KO (−/−) mice would confer a survival disadvantage, as compared with their Cav-1 WT (+/+) and Cav-1 Het (+/−) littermates. A cohort of 180 mice was generated by intercrossing Cav-1 Het (+/−) mating pairs. The resulting cohort consisted of Cav-1 WT (+/+) ($n = 53$), Cav-1 Het (+/−) ($n = 70$), and Cav-1 KO (−/−) ($n = 57$) animals, which were randomly assigned to male and female cages. The mice were then observed over a 2 year period.

Cav-1 null (−/−) mice exhibited an ∼50% reduction in viability at the end of 2 years with major declines in viability occurring from 27 to 65 weeks (Figure 1). Mice that died within this time frame did so suddenly, without any prodromal syndrome (such as cachexia or noticeable changes in behavior). There was no evidence of trauma or dental occlusion, and they appeared well nourished. Also, they did

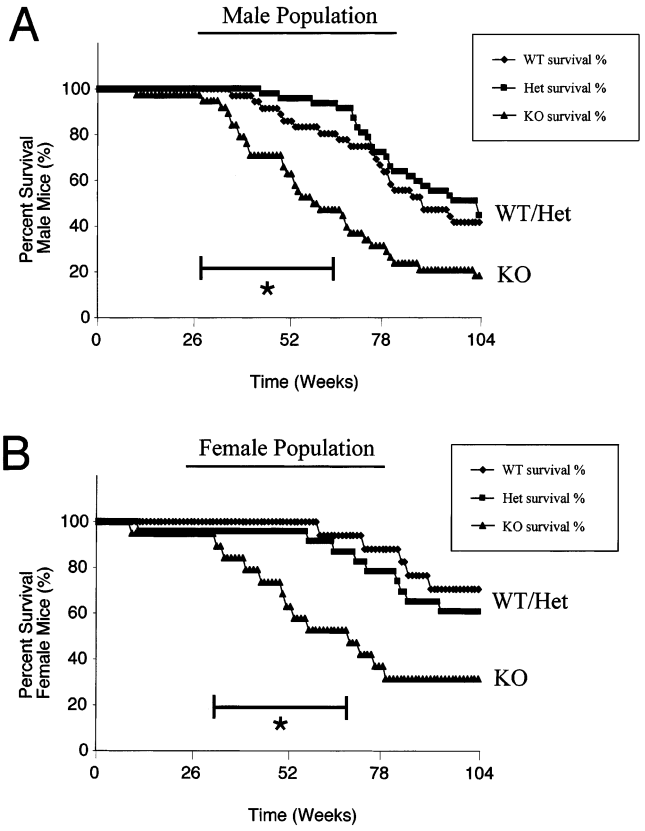

FIGURE 2: Kaplan−Meier survival curves of Cav-1 WT, Het, and KO: male vs female cohorts. A breakdown of the total cohort into male (panel A) and female (panel B) groups demonstrated similar reductions in long-term survival of ∼50%. In addition, both male and female mice experienced marked declines in viability between 27 and 65 weeks (see asterisk). Once again, male and female Cav-1 Het (+/−) mice did not show any changes in long-term survival.

not show ruffling of the fur, labored breathing at rest, or signs of ascites (pancaking). Interestingly, Cav-1 null (−/−) male and female mice both demonstrated similar rates of mortality (Figure 2). As such, the diminished long-term viability of Cav-1 null mice abolished the normal sexual dimorphism in survival, typically seen in wild-type control mice (Figure 3).

A thorough investigation of all major organ systems was undertaken to determine the cause of death in Cav-1 null (−/−) mice. Although necroscopic evaluation of these mice failed to reveal any histological evidence of myocardial infarction, cerebrovascular accident, or malignancy, Cav-1 null (−/−) mice did exhibit progressive worsening of the cardiac and pulmonary defects.

Cardiac Defects. The heart consists of ∼60% cardiac myocytes (that express Cav-3), while the remaining ∼40% is made up of nonmuscle cells, i.e., cardiac fibroblasts, endothelial cells, and smooth muscle cells (that express Cav-1) (*43*, *48*). Recently, two groups have reported that the hearts of Cav-1 null mice are structurally and functionally abnormal at 2−4 months of age (*42*, *43*). Using gated MRI analysis, Cohen et al. demonstrated significant thickening of left and right ventricular walls (*43*). In contrast, Zhao et al. reported a dilated cardiomyopathy, with thinning of the posterior wall and septum (*42*). The presence of both dilated and hypertrophic cardiomyopathy in Cav-1 null (−/−) mice is akin to the dual phenotypes found in the cardiomyopathic hamster

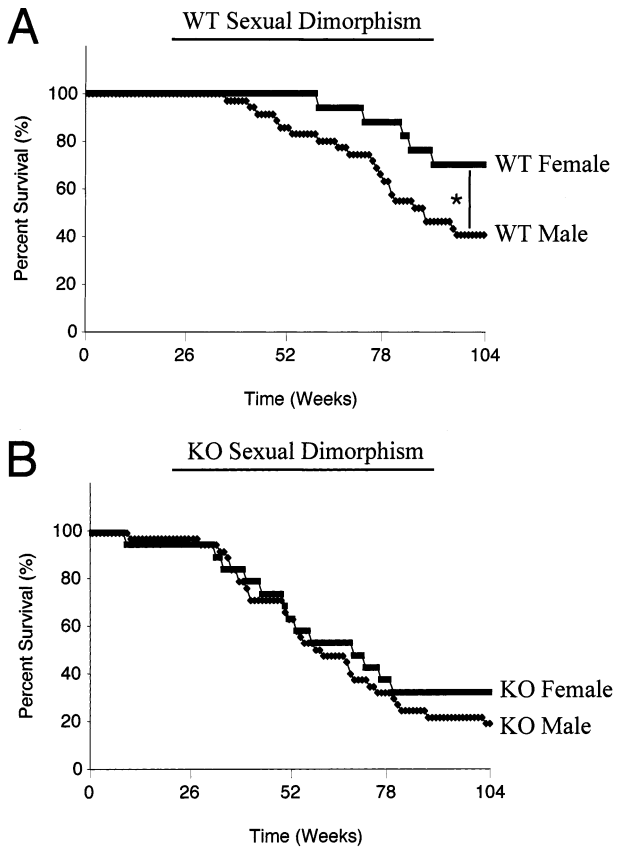

FIGURE 3: Abolition of the normal sexual dimorphism in long-term survival in Cav-1 null (−/−) mice. WT female mice typically experience better long-term survival, as compared with their WT male counterparts, as demonstrated by our WT cohort (panel A). However, genetic ablation of Cav-1 resulted in a loss of this protective effect in females, resulting in similar rates of mortality between male and female Cav-1 null (−/−) mice (panel B).

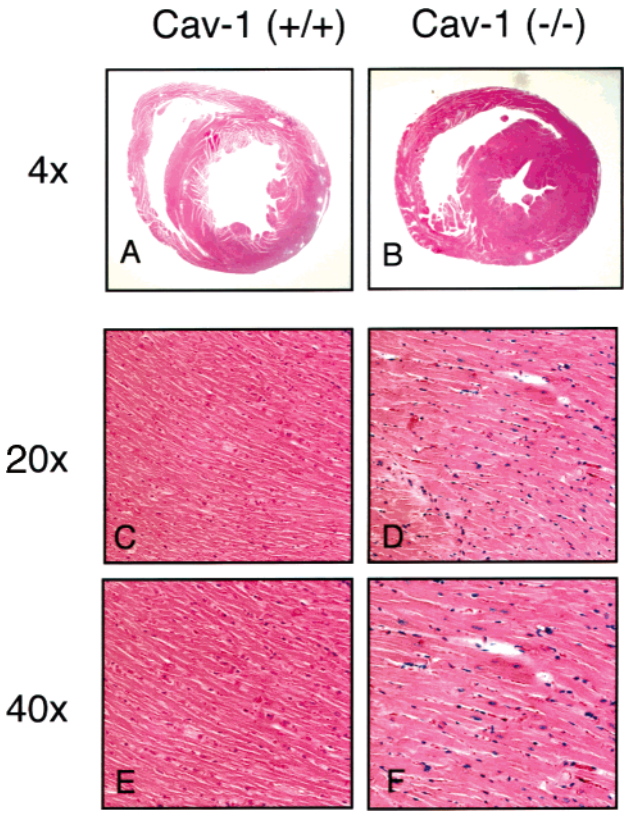

FIGURE 4: Histological examination of 12-month-old Cav-1 KO (−/−) hearts by H and E staining. (A, B) Cav-1 KO (−/−) heart sections revealed profound thickening of the myocardium, in both the left and right ventricles, as compared to their age-matched wild-type counterparts. Note the concentric hypertrophy of the Cav-1 KO (−/−) heart, involving the anterior and posterior walls, and the interventricular septum. (C, D) Examination at 20× magnification demonstrated generalized myocyte hypertrophy and disorganization, which is more advanced than the focal lesions seen in 2- and 4-month-old Cav-1 null (−/−) hearts (*43*). These results suggest that the cardiac hypertrophy is progressive and that mortality may correlate with the degree of cardiac hypertrophy. (E, F) At 40× magnification, cardiac myocyte hypertrophy can be readily appreciated. Accompanying the hypertrophy, enlarged myocellular nuclei and doublet nuclei are observed throughout the myocardium.

model and γ-sarcoglycan knockout mice (*49*, *50*). The variability in disease expression in these animal models may be influenced by the type of anesthetic used or by genetic modifier loci (*43*). However, both groups noted a functional impairment of young Cav-1 null (−/−) mouse hearts using transthoracic echocardiography as evidenced by diminished fractional shortening, a measure of cardiac systolic functioning (*42*, *43*).

Histological analysis revealed focal areas of hypertrophy, disarray, and degeneration of cardiac myocytes with interstitial/perivascular fibrosis in 2- and 4-month-old Cav-1 null (−/−) hearts (*43*). Cav-1 null (−/−) cardiac fibroblasts exhibited hyperactivation of the p42/44 MAP kinase cascade in fibrotic lesions within intact hearts, as well as in isolated cultured cardiac fibroblasts (*43*). This is consistent with numerous previous reports demonstrating that Cav-1 acts as a negative regulator of the p42/44 MAP kinase cascade (*43*). Thus, it appears that loss of caveolin-1 expression in cardiac fibroblasts leads to p42/44 MAP kinase hyperactivation and interstitial fibrosis, contributing to the development of cardiac hypertrophy.

To determine if the cause of death in these mice was related to cardiac hypertrophy, the hearts from 12-month-old Cav-1 KO (−/−) mice were sectioned and examined histologically. Hearts from Cav-1 WT (+/+) littermate mice of the same age were used as controls for comparison. It is important to note that virtually identical results were obtained with Cav-1 KO (−/−) mice that were found dead and subjected to necropsy.

As shown in Figure 4A,B, 12-month-old Cav-1 KO (−/−) mice show profound thickening of the myocardium in both the left and right ventricles, as compared to their wild-type counterparts. Examination at higher magnifications (20× and 40×) demonstrated generalized myocyte hypertrophy and disorganization (Figure 4C,D), which are clearly more advanced than the focal lesions we previously reported in 2- and 4-month-old Cav-1 null (−/−) mice (*43*). At 40× magnification, enlarged myocellular nuclei and double nuclei are apparent within the myocardium (Figure 4E,F).

It is now well accepted that cardiac fibroblasts play a significant role in the process of cardiac structural remodeling and cardiac hypertrophy. Cardiac fibroblasts maintain the integrity of the myocardium by producing the extracellular matrix, as well as a multitude of growth factors and cytokines (*51*). The histopathology of Cav-1 KO hearts is consistent with the structural rearrangements characteristic of cardiac remodeling. Reactive fibrosis adversely affects cardiac function by several mechanisms: (i) accumulation of type I collagen stiffens ventricular tissue, leading to decreased

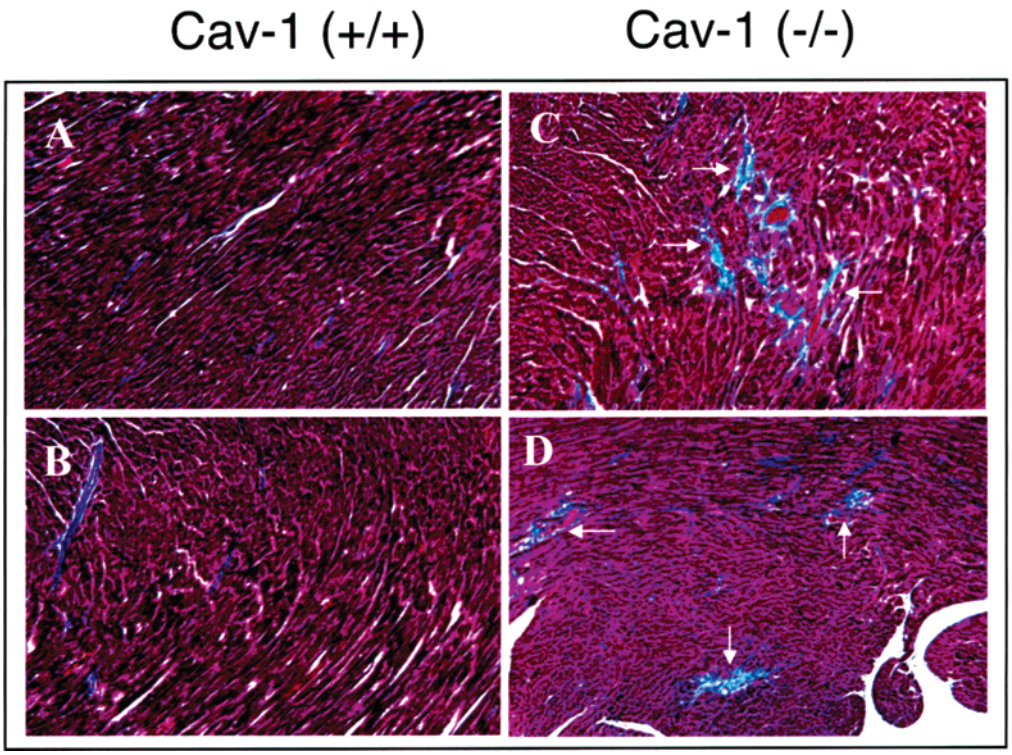

FIGURE 5: Histological examination of 12-month-old Cav-1 KO (−/−) hearts by trichrome staining. Paraffin-embedded mouse hearts were sectioned and subjected to trichrome staining to identify possible areas of fibrosis. Interestingly, the hearts of 12-month-old Cav-1 null (−/−) mice show a significant increase in trichrome staining throughout the myocardium and particularly around large vessels (interstitial and perivascular fibrosis; panels C and D). Arrows point at the areas of blue-green staining. In contrast, the hearts of Cav-1 (+/+) wild-type mice show much less detectable fibrosis, if any (panels A and B).

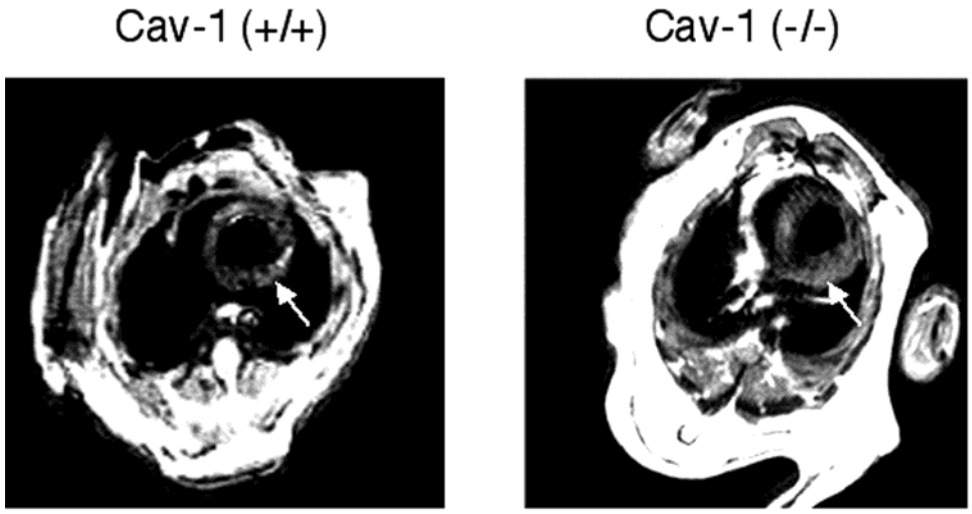

FIGURE 6: Gated MRI analysis of Cav-1 KO (−/−) hearts at 12 months of age. We investigated hearts of older Cav-1 null mice using a noninvasive technique, gated magnetic resonance imaging (MRI). Note that Cav-1 null mice demonstrate significant left ventricular (LV) wall thickening (~36% thicker; see arrows), as compared to wild-type control mice. See Table 1 for detailed quantitation.

contractility; (ii) intermyocellular fibrosis impedes electrical coupling, leading to inefficient, or even abnormal, conduction; and (iii) fibrosis impairs oxygen diffusion, leading to myocellular hypoxia and/or ischemia (*51*). Consistent with our previous observations at 2 and 4 months of age, trichrome staining of the myocardium reveals a significant increase in fibrosis in 12-month-old Cav-1 KO (−/−) mice (Figure 5).

We next investigated the hearts of older Cav-1 null mice using a noninvasive technique, gated magnetic resonance imaging (MRI). Current MRI technology provides the most accurate and reliable noninvasive method of quantitatively determining several parameters in the murine heart, especially right ventricular (RV) chamber size (*52*). Cardiac gating allows for the timing of images that correspond to systolic and diastolic portions of the cardiac cycle, thus allowing for measurements of the fully dilated and fully contracted ventricular chamber.

Using this technique, we examined the hearts of 12-month-old Cav-1 null (−/−) mice and age-matched controls for several parameters (Figure 6, Table 1). We found that, at 12 months of age, Cav-1 null mice demonstrate significant left ventricular (LV) wall thickening (~36% thicker), as com-

Table 1: MRI Analysis of the Hearts of WT and Cav-1 KO Mice at 4 and 12 Months of Age

genotype	age (months)	left ventricular wall thickness (mm)	right ventricular internal diameter (mm)
wild type	4[b]	0.95 ± 0.04	1.48 ± 0.05
Cav-1 null	4[b]	1.12 ± 0.07[a]	2.52 ± 0.15[a]
wild type	12	1.09 ± 0.11	1.56 ± 0.21
Cav-1 null	12	1.48 ± 0.12[a]	1.95 ± 0.13[a]

[a] $p < 0.05$; $n \geq 4$ for each experimental group. [b] Comparative values reproduced from Cohen et al. (*43*).

pared to wild-type control mice. Interestingly, the right ventricular (RV) chamber size of Cav-1 null mice is ~25% larger than in the wild-type mice of the same age.

Results obtained with younger mice (4 months of age) are shown for comparison [Table 1 (*43*)]. At 4 months of age, Cav-1 null mice demonstrate an ~18% increase in LV wall thickness and an ~70% larger RV chamber when compared to age-matched wild-type mice. Thus, in Cav-1 null mice, the observed left ventricular (LV) wall thickening is clearly progressive, while RV chamber size decreases with increasing age.

While gated cardiac MRI provides a significant means by which measurements of several cardiac parameters can be made, this technique is limited in that it cannot give the most accurate measurements of dynamic parameters, such as systolic function. Therefore, to more thoroughly evaluate the cardiac defects observed in Cav-1 null (−/−) mice, we next performed transthoracic echocardiography on wild-type and Cav-1 null (−/−) mice at 12 months of age.

As seen in Table 2, results obtained by echocardiography show that 12-month-old Cav-1 null (−/−) mice exhibit significant left ventricular hypertrophy with increases of ~51% in intraventricular septal thickness, posterior wall thickness, and LV wall thickness during diastole, when compared to age-matched wild-type control mice.

At 12 months of age Cav-1 null (−/−) mice also demonstrate a significant reduction in left ventricular systolic function, as evidenced by decreased fractional shortening (Table 2). Cav-1 null (−/−) mice show an ~29% decrease in fractional shortening, when compared to age-matched wild-type controls. Thus, consistent with concentric left ventricular hypertrophy, 12-month-old Cav-1 null (−/−) mice demonstrate progressive increases in LV wall thickness with normal left ventricular end-diastolic dimension and reduced left ventricular systolic function.

The onset of sudden death in Cav-1 null (−/−) mice in the absence of cerebrovascular accident, myocardial infarction, or massive pulmonary embolus is consistent with the sudden cardiac death syndrome that is associated with hypertrophic cardiomyopathy. Hypertrophic cardiomyopathy is classically associated with arrythmias and premature sudden death secondary to the progressive disorganization of cardiac tissue (*53*, *54*). Another possible mechanism of sudden cardiac death syndrome in left ventricular hypertrophy could be thrombotic or ischemic events, due to hypercoagulability, endothelial dysfunction, or poor oxygen diffusion (*54*). Future workup of these mice should include prolonged ECG monitoring to assess the presence of possible rhythm abnormalities at rest and during exercise.

Pulmonary Defects. Another tissue with notably high caveolin-1 expression is the lung, which is particularly abundant in endothelial cells and type I pneumocytes (*55*). Several groups have now independently generated Cav-1-deficient mice and have reported marked defects in lung development. Histological examination of Cav-1 null (−/−) lung tissue revealed marked hypercellularity resulting in thickening of alveolar septa (*42*, *45*, *56*, *57*). To identify the cell population responsible for the hypercellular phenotype, specific markers for endothelial cells, type I pneumocytes, and alveolar macrophages were examined using immunohistochemistry. Of the antibodies used, the endothelial marker Flk-1 (VEGF receptor) displayed a significant increase in cellular staining in Cav-1 null (−/−) lung sections (*45*, *56*). Furthermore, staining with Ki67, a marker for cellular proliferation, demonstrated a dramatic increase in the number of proliferating cells (*45*).

Zhao and colleagues have recently reported that Cav-1-deficient (−/−) mice exhibit pulmonary hypertension, resulting in right ventricular hypertrophy and dilation, as determined by weight and histology measurements (*42*). Hemodynamic data revealed significant increases in RV contractility and diastolic function. Consistent with pulmonary hypertension, pulmonary artery pressures in Cav-1 (−/−) null mice were found to be ~90% higher than their wild-type counterparts, and LV/RV ratios were decreased with no outflow tract obstructions and normal left-sided heart pressures. This suggests that the pulmonary hypertension is independent of the left ventricular heart defects but rather is secondary to an intrinsic defect of the lungs. Cav-1 null (−/−) mice also exhibited signs of cor pulmonale, with increases in liver/body weight measurements suggestive of severe right-sided failure (*42*).

In the present study, lungs from 12-month-old Cav-1 KO (−/−) mice were examined morphologically. On gross examination, they appeared hyperemic. Histological examination revealed advanced alveolar septal thickening, increased inflammatory infiltrates, and reactive endothelial cell proliferation (Figure 7). In addition, the alveolar spaces were filled with extravasated red blood cells. It is important to note that virtually identical results were obtained with Cav-1 KO (−/−) mice that were found dead and subjected to necropsy.

Right ventricle (RV) wet weight-to-body weight ratios were measured to determine the degree of right heart strain (Figure 8). At 12 months of age, the Cav-1 (−/−) RV-to-body weight ratio [1.91 ± 0.39 (mg/g); $n = 5$] was found to be >2-fold elevated, as compared with their Cav-1 (+/+)

Table 2: Echocardiographic Analysis of WT and Cav-1 KO Mice at 12 Months of Age[a]

genotype	end diastolic diameter (mm)	end systolic diameter (mm)	intraventricular septal thickness (mm)	posterior wall thickness (mm)	wall thickness diastole (mm)	relative wall thickness (ratio)	fractional shortening (%)
wild type	3.23 ± 0.15	1.51 ± 0.15	0.70 ± 0.01	0.75 ± 0.02	0.73 ± 0.01	0.46 ± 0.02	53.9 ± 2.5
Cav-1 null	2.78 ± 0.12[b]	1.64 ± 0.14	1.09 ± 0.03[b]	1.10 ± 0.03[b]	1.10 ± 0.02[b]	0.80 ± 0.04[b]	41.6 ± 3.8[b]

[a] $n \geq 7$ for each experimental group. [b] $p < 0.03$.

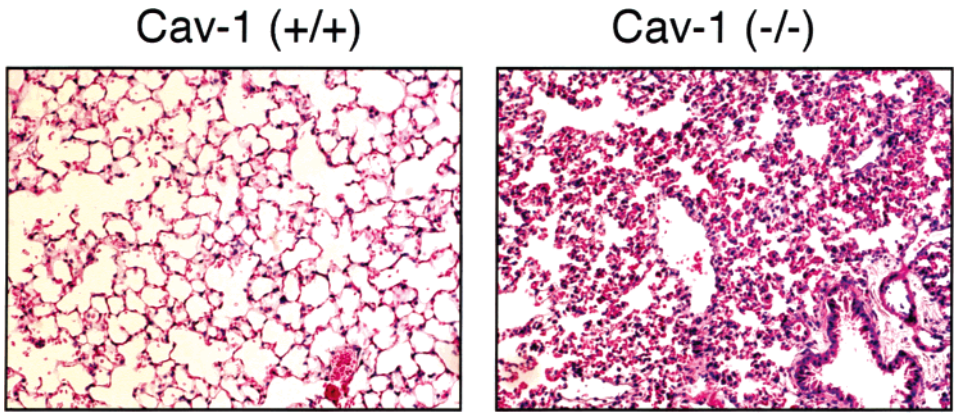

FIGURE 7: Histological examination of 12-month-old Cav-1 KO (−/−) lung tissue by H and E staining. Lungs were harvested from 12-month-old Cav-1 KO (−/−) mice, paraffin-embedded, and sectioned. Interestingly, histological examination revealed advanced alveolar septal thickening and increased inflammatory infiltrates, with reactive endothelial cell proliferation. In addition, the alveolar spaces were filled with extravasated red blood cells. Note that much of the typical alveolar structure has been replaced by inflammatory cells and proliferating endothelial-like cells.

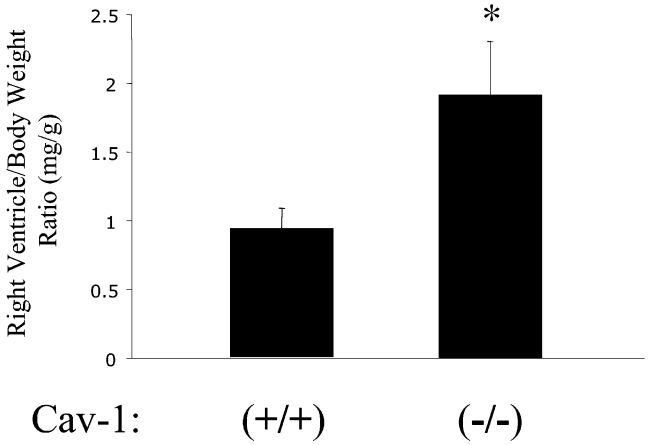

FIGURE 8: Degree of right heart strain in 12-month-old Cav-1 KO (−/−) mice. At 12 months of age, right ventricle wet weight-to-body weight ratios (mg/g) were measured. Note that the Cav-1 (−/−) RV-to-body weight ratio is >2-fold elevated, as compared with Cav-1 (+/+) wild-type mice. An asterisk denotes statistical significance ($n = 5$ for each experimental group; $p < 0.01$).

wild-type counterparts [0.93 ± 0.15 (mg/g); $n = 5$; $p < 0.01$]. In addition, at 12 months of age, the liver-to-body weight ratios demonstrated an ~20% increase in Cav-1 null (−/−) mice, consistent with severe right-sided heart failure.

Severe pulmonary hypertension is associated with high morbidity and mortality and is characterized by marked derangements of angiogenesis in the pulmonary vasculature (*58*−*60*). This aberrant angiogenesis of endothelial progenitor-like cells occurs due to inactivation of certain tumor suppressor genes, leading to the dysregulated expression of angiogenesis-related molecules, such as VEGF and VEGFR-2 (*59*, *60*). The consequence is a loss of endothelial monolayer growth resulting in the formation of intravascular "tumorlets" or plexiform lesions (*60*). These physiologic and histopathologic data demonstrate the importance of Cav-1 in maintaining normal lung physiology and pulmonary vascular angiogenesis.

Consistent with pulmonary hypertension, Cav-1 null (−/−) mice exhibited an impairment of exercise tolerance, as compared with wild-type littermates (*45*, *56*). Also, the aberrant growth of endothelial-like progenitor cells expressing angiogenesis-related proteins (such as Flk-1) confirms previous work illustrating the critical role of Cav-1 in endothelial cell proliferation and maturation (*55*, *61*). Considering the severity of the pulmonary hypertension in Cav-1 null (−/−) mice, acute respiratory failure compounded with right-sided heart failure is another possible cause of reduced viability.

CONCLUSIONS

In summary, we show here that Cav-1 null (−/−) mice exhibit an ~50% reduction in viability at the end of 2 years, with the major declines in viability occurring from 27 to 65 weeks of age. This dramatic reduction in life span appears to be secondary to a combination of pulmonary fibrosis, pulmonary hypertension, and cardiac hypertrophy. Thus, Cav-1 null (−/−) mice may represent a new animal model to study the pathogenesis of progressive hypertrophic cardiomyopathy and sudden cardiac death syndrome.

REFERENCES

1. Smart, E., Ying, Y.-S., Conrad, P., and Anderson, R. G. W. (1994) *J. Cell Biol. 127*, 1185−1197.
2. Murata, M., Peranen, J., Schreiner, R., Weiland, F., Kurzchalia, T., and Simons, K. (1995) *Proc. Natl. Acad. Sci., U.S.A. 92*, 10339−10343.
3. Smart, E. J., Ying, Y.-s., Donzell, W. C., and Anderson, R. G. W. (1996) *J. Biol. Chem. 271*, 29427−29435.
4. Monier, S., Dietzen, D. J., Hastings, W. R., Lublin, D. M., and Kurzchalia, T. V. (1996) *FEBS Lett. 388*, 143−149.
5. Razani, B., Combs, T. P., Wang, X. B., Frank, P. G., Park, D. S., Russell, R. G., Li, M., Tang, B., Jelicks, L. A., Scherer, P. E., and Lisanti, M. P. (2001) *J. Biol. Chem. 277*, 8635−8647.
6. van Meer, G. (2001) *J. Cell Biol. 152*, F29−F34.
7. Hulit, J., Bash, T., Fu, M., Galbiati, F., Albanese, C., Sage, D. R., Schlegel, A., Zhurinsky, J., Shtutman, M., Ben-Ze'ev, A., Lisanti, M. P., and Pestell, R. G. (2000) *J. Biol. Chem. 275*, 21203−21209.
8. Galbiati, F., Volonte, D., Liu, J., Capozza, F., Frank, P. G., Zhu, L., Pestell, R. G., and Lisanti, M. P. (2001) *Mol. Biol. Cell 12*, 2229−2244.
9. Liu, J., Lee, P., Galbiati, F., Kitsis, R. N., and Lisanti, M. P. (2001) *Am. J. Physiol. Cell Physiol. 280*, C823−C835.
10. Schlegel, A., Pestell, R. G., and Lisanti, M. P. (2000) *Front. Biosci. 5*, D929−D937.
11. van Meer, G., Stelzer, E. H. K., Wijnaendts-van Resandt, R. W., and Simons, K. (1987) *J. Cell Biol. 105*, 1623−1635.
12. Fiedler, K., Kobayashi, T., Kurzchalia, T., and Simons, K. (1993) *Biochemistry 32*, 6365−6373.
13. Hanada, K., Nishijima, M., Akamatsu, Y., and Pagano, R. E. (1995) *J. Biol. Chem. 270*, 6254−6260.

14. Simons, K., and Toomre, D. (2000) *Nat. Rev. Mol. Cell Biol. 1*, 31−39.
15. Lisanti, M. P., Scherer, P., Tang, Z.-L., and Sargiacomo, M. (1994) *Trends Cell Biol. 4*, 231−235.
16. Shenoy-Scaria, A. M., Dietzen, D. J., Kwong, J., Link, D. C., and Lublin, D. M. (1994) *J. Cell Biol. 126*, 353−363.
17. Robbins, S. M., Quintrell, N. A., and Bishop, M. J. (1995) *Mol. Cell. Biol. 15*, 3507−3515.
18. Liu, J., Garcia-Cardena, G., and Sessa, W. C. (1996) *Biochemistry 35*, 13277−13281.
19. Lee, H., Woodman, S. E., Engelman, J. A., Volonte, D., Galbiati, F., Kaufman, H. L., Lublin, D. M., and Lisanti, M. P. (2001) *J. Biol. Chem. 276*, 35150−35158.
20. Sargiacomo, M., Scherer, P. E., Tang, Z.-L., Kubler, E., Song, K. S., Sanders, M. C., and Lisanti, M. P. (1995) *Proc. Natl. Acad. Sci., U.S.A. 92*, 9407−9411.
21. Li, S., Okamoto, T., Chun, M., Sargiacomo, M., Casanova, J. E., Hansen, S. H., Nishimoto, I., and Lisanti, M. P. (1995) *J. Biol. Chem. 270*, 15693−15701.
22. Garcia-Cardena, G., Oh, P., Liu, J., Schnitzer, J. E., and Sessa, W. C. (1996) *Proc. Natl. Acad. Sci., U.S.A. 93*, 6448−6453.
23. Shaul, P. W., Smart, E. J., Robinson, L. J., German, Z., Yuhanna, I. S., Ying, Y., Anderson, R. G. W., and Michel, T. (1996) *J. Biol. Chem. 271*, 6518−6522.
24. Song, K. S., Li, S., Okamoto, T., Quilliam, L., Sargiacomo, M., and Lisanti, M. P. (1996) *J. Biol. Chem. 271*, 9690−9697.
25. Engelman, J. A., Lee, R. J., Karnezis, A., Bearss, D. J., Webster, M., Siegel, P., Muller, W. J., Windle, J. J., Pestell, R. G., and Lisanti, M. P. (1998) *J. Biol. Chem. 273*, 20448−20455.
26. Song, K. S., Sargiacomo, M., Galbiati, F., Parenti, M., and Lisanti, M. P. (1997) *Cell. Mol. Biol. (Noisy-le-Grand) 43*, 293−303.
27. Park, D. S., Lee, H., Frank, P. G., Razani, B., Nguyen, A. V., Parlow, A. F., Russell, R. G., Hulit, J., Pestell, R. G., and Lisanti, M. P. (2002) *Mol. Biol. Cell 13*, 3416−3430.
28. Glenney, J. R. (1989) *J. Biol. Chem. 264*, 20163−20166.
29. Anderson, R. G. W. (1998) *Annu. Rev. Biochem. 67*, 199−225.
30. Koleske, A. J., Baltimore, D., and Lisanti, M. P. (1995) *Proc. Natl. Acad. Sci. U.S.A. 92*, 1381−1385.
31. Engelman, J. A., Wycoff, C. C., Yasuhara, S., Song, K. S., Okamoto, T., and Lisanti, M. P. (1997) *J. Biol. Chem. 272*, 16374−16381.
32. Galbiati, F., Volonté, D., Engelman, J. A., Watanabe, G., Burk, R., Pestell, R., and Lisanti, M. P. (1998) *EMBO J. 17*, 6633−6648.
33. Lee, S. W., Reimer, C. L., Oh, P., Campbel, l. D. B., and Schnitzer, J. E. (1998) *Oncogene 16*, 1391−1397.
34. Zhang, W., Razani, B., Altschuler, Y., Bouzahzah, B., Mostov, K. E., Pestell, R. G., and Lisanti, M. P. (2000) *J. Biol. Chem. 275*, 20717−20725.
35. Engelman, J. A., Zhang, X. L., and Lisanti, M. P. (1998) *FEBS Lett. 436*, 403−410.
36. Engelman, J. A., Zhang, X. L., and Lisanti, M. P. (1999) *FEBS Lett. 448*, 221−230.
37. Hayashi, K., Matsuda, S., Machida, K., Yamamoto, T., Fukuda, Y., Nimura, Y., Hayakawa, T., and Hamaguchi, M. (2001) *Cancer Res 61*, 2361−2364.
38. Minetti, C., Sotogia, F., Bruno, C., Scartezzini, P., Broda, P., Bado, M., Masetti, E., Mazzocco, P., Egeo, A., Donati, M. A., Volonte', D., Galbiati, F., Cordone, G., Bricarelli, F. D., Lisanti, M. P., and Zara, F. (1998) *Nat. Genet. 18*, 365−368.
39. Lee, H., Park, D. S., Razani, B., Russell, R. G., Pestell, R. G., and Lisanti, M. P. (2002) *Am. J. Pathol. 161*, 1357−1369.
40. Galbiati, F., Engelman, J. A., Volonte, D., Zhang, X. L., Minetti, C., Li, M., Hou, H., Jr., Kneitz, B., Edelmann, W., and Lisanti, M. P. (2001) *J. Biol. Chem. 276*, 21425−21433.
41. Park, D. S., Woodman, S. E., Schubert, W., Cohen, A. W., Frank, P. G., Chandra, M., Shirani, J., Razani, B., Tang, B., Jelicks, L. A., Factor, S. M., Weiss, L. M., Tanowitz, H. B., and Lisanti, M. P. (2002) *Am. J. Pathol. 160*, 2207−2217.
42. Zhao, Y. Y., Liu, Y., Stan, R. V., Fan, L., Gu, Y., Dalton, N., Chu, P. H., Peterson, K., Ross, J., Jr., and Chien, K. R. (2002) *Proc. Natl. Acad. Sci. U.S.A. 99*, 11375−11380.
43. Cohen, A. W., Park, D. S., Woodman, S. E., Williams, T. M., Chandra, M., Shirani, J., Pereira de Souza, A., Kitsis, R. N., Russell, R. G., Weiss, L. M., Tang, B., Jelicks, L. A., Factor, S. M., Shtutin, V., Tanowitz, H. B., and Lisanti, M. P. (2003) *Am. J. Physiol. Cell Physiol. 284*, C457−C474.
44. Cohen, A. W., Razani, B., Wang, X. B., Combs, T. P., Williams, T. M., Scherer, P. E., and Lisanti, M. P. (2003) *Am. J. Physiol. Cell Physiol. 285*, C222−C235.
45. Razani, B., Engelman, J. A., Wang, X. B., Schubert, W., Zhang, X. L., Marks, C. B., Macaluso, F., Russell, R. G., Li, M., Pestell, R. G., Di Vizio, D., Hou, H., Jr., Kneitz, B., Lagaud, G., Christ, G. J., Edelmann, W., and Lisanti, M. P. (2001) *J. Biol. Chem. 276*, 38121−38138.
46. Williams, T. M., Cheung, M. W., Park, D. S., Razani, B., Cohen, A. W., Muller, W. J., Di Vizio, D., Chopra, N. G., Pestell, R. G., and Lisanti, M. P. (2003) *Mol. Biol. Cell 14*, 1027−1042.
47. Schiller, N. B., Shah, P. M., Crawford, M., DeMaria, A., Devereux, R., Feigenbaum, H., Gutgesell, H., Reichek, N., Sahn, D., Schnittger, I., et al. (1989) *J. Am. Soc. Echocardiogr. 2*, 358−367.
48. MacKenna, D., Summerour, S. R., and Villarreal, F. J. (2000) *Cardiovasc. Res. 46*, 257−263.
49. Hack, A. A., Groh, M. E., and McNally, E. M. (2000) *Microsc. Res. Tech. 48*, 167−180.
50. Hack, A. A., Ly, C. T., Jiang, F., Clendenin, C. J., Sigrist, K. S., Wollmann, R. L., and McNally, E. M. (1998) *J. Cell Biol. 142*, 1279−1287.
51. Manabe, I., Shindo, T., and Nagai, R. (2002) *Circ. Res. 91*, 1103−1113.
52. Weiss, R. G. (2001) *Circ. Res. 88*, 550−551.
53. Maron, B. J. (2002) *Circulation 106*, 2419−2421.
54. Tin, L. L., Beevers, D. G., and Lip, G. Y. (2002) *Curr. Cardiol. Rep. 4*, 449−457.
55. Liu, J., Razani, B., Tang, S., Terman, B. I., Ware, J. A., and Lisanti, M. P. (1999) *J. Biol. Chem. 274*, 15781−15785.
56. Drab, M., Verkade, P., Elger, M., Kasper, M., Lohn, M., Lauterbach, B., Menne, J., Lindschau, C., Mende, F., Luft, F. C., Schedl, A., Haller, H., and Kurzchalia, T. V. (2001) *Science 293*, 2449−2452.
57. Cao, G., Yang, G., Timme, T. L., Saika, T., Truong, L. D., Satoh, T., Goltsov, A., Park, S. H., Men, T., Kusaka, N., Tian, W., Ren, C., Wang, H., Kadmon, D., Cai, W. W., Chinault, A. C., Boone, T. B., Bradley, A., and Thompson, T. C. (2003) *Am. J. Pathol. 162*, 1241−1248.
58. Haworth, S. G. (2002) *Heart 88*, 658−664.
59. Olschewski, H., Rose, F., Grunig, E., Ghofrani, H. A., Walmrath, D., Schulz, R., Schermuly, R., Grimminger, F., and Seeger, W. (2001) *J. Lab. Clin. Med. 138*, 367−377.
60. Tuder, R. M., and Voelkel, N. F. (2002) *Antioxid. Redox Signaling 4*, 833−843.
61. Liu, J., Wang, X. B., Park, D. S., and Lisanti, M. P. (2002) *J. Biol. Chem. 277*, 10661−10668.

BI0356348